Available online at www.sciencedirect.com

SciVerse ScienceDirect

Scripta Materialia 66 (2012) 943–946

Scripta MATERIALIA

www.elsevier.com/locate/scriptamat

Copper precipitation in cobalt-alloyed precipitation-hardened stainless steel

Arpana S. Murthy,[a,*] Julia E. Medvedeva,[b] Dieter Isheim,[c] Simon L. Lekakh,[a] Von L. Richards[a] and David C. Van Aken[a]

[a]*Department of Materials Science and Engineering, Missouri University of Science and Technology, Rolla, MO 65401, USA*
[b]*Department of Physics, Missouri University of Science and Technology, Rolla, MO 65401, USA*
[c]*Northwestern University Center for Atom-Probe Tomography, Northwestern University, Evanston, IL 60208-3108, USA*

Received 7 February 2012; revised 22 February 2012; accepted 23 February 2012
Available online 1 March 2012

The influence of cobalt addition on precipitation of copper in a high-strength stainless steel was investigated using three-dimensional atom probe tomography. A decrease in copper precipitate size with narrowed distribution was observed in cobalt-containing steel. The concentration profile across the precipitate–matrix interface indicated rejection of cobalt atoms from the copper precipitates. This behavior was explained with first-principles calculations using energy-minimization criterion.

Keywords: 3DAP; Stainless steels; First-principle electron theory; Casting; Precipitation

Precipitation-hardened (PH) steels are classified as such because they derive strength from nanometer-size precipitates formed during thermal aging. The stainless steel designated 17-4 PH is a low-carbon martensitic alloy that is precipitation hardened by Cu. Early works on Fe–Cu steel indicate that the peak hardness is achieved when the Cu precipitates are coherent (body-centered cubic (bcc)) within the martensite matrix [1–3]. Cu precipitates have been observed in high-strength steels using atom probe tomography (APT) [4–9]. Recently, using APT, it has been reported that the concentration of Cu in these Cu precipitates is 50–70 at.% [6–8,10–12]. An enrichment of Ni and Mn at the Cu precipitate–matrix interface has also been observed [7,8,10]. These studies [4–12] demonstrate that APT is an effective technique for estimating the precipitate size, morphology, and composition across the precipitate–matrix interface, and thereby assists in further understanding of precipitation in steels.

Co addition to martensitic steel has been reported to increase strength by inhibition of dislocation recovery and reduction in martensitic block size, thus producing a higher secondary hardening [13]. Co addition to wrought 17-4 PH steel has led to an increase in hardness [14,15]. Recently, the authors observed an increase in strength and toughness by Co addition to cast 17-4 PH steel [16]; however, the effect of Co on the Cu precipitation in cast 17-4 PH steel was not fully understood.

In the present work, APT and first-principles investigation have been employed to understand the effect of Co on Cu precipitate formation.

Three cast alloys, 17-4 PH with no Co, and 17-4 PH alloyed with 3 wt.% and 7 wt.% Co additions, were melted in a 45 kg coreless induction furnace under an inert gas (Ar) cover protection and cast into no-bake molds with a top riser to obtain Y-blocks measuring 18 mm × 130 mm × 60 mm, and into ceramic shell molds preheated to 1253 K to produce tensile specimens. Chemical analysis of each heat was obtained using an arc spectrometer ARL 4460, a LECO TC 500 analyzer to measure oxygen and nitrogen, and a LECO CS 600 analyzer to determine carbon and sulfur (see Table 1).

The specimens of 0 wt.% Co and 7 wt.% Co steels were homogenized for 10.5 h at 1473 K, and those of 3 wt.% Co steel were homogenized for 4 h at 1473 K, to minimize the lath packet size, delta ferrite and segregation in the microstructure, as described elsewhere [16]. Next, these specimens were solution treated at 1323 K for 1 h and quenched into a salt bath, maintained at 423 K. The 0 wt.% Co and 3 wt.% Co specimens were peak aged at 755 K for 75 min; the 7 wt.% Co specimen was peak aged for 90 min [16]. The room temperature tensile and Charpy V-notch properties of these alloys

* Corresponding author. Tel.: +1 573 341 7886; e-mail: asmr52@mst.edu

1359-6462/$ - see front matter © 2012 Acta Materialia Inc. Published by Elsevier Ltd. All rights reserved.
doi:10.1016/j.scriptamat.2012.02.039

Table 1. Chemistry of the alloys studied.

Alloy	Unit	Chemical composition													
		C	Mn	P	S	Si	Cu	Ni	Cr	V	Nb	Co	O	N	Fe
0 wt.% Co	wt.%	0.042	0.41	0.02	0.01	0.81	2.95	3.88	15.74	0.07	0.29	0.06	0.02	0.02	Bal
	at.%	0.19	0.41	0.04	0.02	1.59	2.55	3.63	16.64	0.08	0.17	0.06	0.07	0.06	Bal
3 wt.% Co	wt.%	0.035	0.42	0.02	0.01	1.00	2.83	3.71	15.27	0.07	0.29	2.79	0.01	0.01	Bal
	at.%	0.16	0.42	0..04	0.02	1.96	2.45	3.48	16.15	0.08	0.17	2.60	0.05	0.05	Bal
7 wt.% Co	wt.%	0.035	0.40	0.02	0.02	1.01	2.67	3.45	14.64	0.06	0.26	6.94	0.01	0.02	Bal
	at.%	0.16	0.40	0.04	0.03	1.98	2.31	3.24	15.51	0.06	0.15	6.49	0.05	0.07	Bal

Bal = balance.

with 95% confidence limits are reported in Table 2 [16]. It was observed that addition of Co led to an improvement in strength as well as toughness [16].

Specimens of 0.3 mm × 0.3 mm × 10 mm were cut from peak-aged blanks, and tips for APT were prepared by electropolishing at room temperature in two steps: initially with 10% perchloric acid in acetic acid at 15–17 V DC, and final polishing using 2% perchloric acid in butoxyethanol at 13–14 V DC. The specimens were analyzed using a local electrode atom probe LEAP4000XSi tomograph manufactured by Cameca, Madison, WI (formerly Imago Scientific Instruments). The analyses were done with a 500 kHz pulse repetition frequency, 50 pJ pulse energy, specimen temperature of 40 K, and a 1% evaporation rate. IVAS 3.4 software was used to perform an atom-by-atom 3-D reconstruction of the data sets and data analysis [17]. To calculate proximity histogram [18] concentration profiles, the Cu-rich precipitates were discriminated by a 10% Cu isoconcentration surface, obtained with a voxel size of 1 nm and delocalization of 3 nm. Approximately 2000 precipitates were analyzed in each specimen. To take potential distortion [19] of the precipitates in the reconstruction into account, the precipitate radius was calculated from the number of atoms in a given precipitate, and not measured directly from the reconstruction. The cluster search method with maximum separation algorithm [20] was used to calculate the number of atoms and volume of the precipitates. The minimum number of atoms defining a cluster, $N_{\min}$, was 50 atoms and the critical distance, $d_{\max}$, between solute atoms was 0.6 nm. The average volume equivalent radius of these spherical Cu precipitates calculated using Eq. (1) were 2.26 ± 0.016 nm in 0 wt.% Co, 2.15 ± 0.014 nm in 3 wt.% Co, and 2.18 ± 0.014 nm in 7 wt.% Co 17-4 PH steel.

$$V = \frac{n}{\rho_{atomic} \cdot f} \tag{1}$$

For Eq. (1), n is the number of atoms detected for each Cu precipitate by maximum separation algorithm, V is the volume of the precipitate, ρ_{atomic} is the atomic density of bcc iron, and f is the overall detection and reconstruction efficiency, estimated to be 0.5 [7]. Figure 1 presents a representative volume of 40 nm × 40 nm × 40 nm for all three alloys investigated, with the Cu precipitates discriminated by a 10 at.% Cu isoconcentration surface.

The probability of two data sets being different from each other with statistical significance can be determined using a statistical t-test analysis. The unequal variance t-test analysis was conducted between the Cu precipitate radii of 0 wt.% Co and 3 wt.% Co steel, and 3 wt.% Co and 7 wt.% Co steel. The probability of the radii data of 0 wt.% Co and 3 wt.% Co steel being different is >0.99 and that for 3 wt.% Co and 7 wt.% Co is >0.94, thereby indicating that the data sets were different to a statistically significant extent. Figure 2 presents the Cu precipitate size distribution with respect to radii normalized by the mean radius for each of the three alloys. The standard deviation in the radius of the precipitates is 0.715 nm in 0 wt.% Co steel, 0.643 nm in 3 wt.% Co steel and 0.637 nm in 7 wt.% Co steel. It is observed that the size distribution is narrower in the steels with Co as compared to the steel with no Co.

The isoconcentration surfaces outlined at 10 at.% Cu delineate all areas with a Cu concentration greater than 10 at.%. The proximity histogram concentration profiles of Fe, Cu, Cr, Ni, Co, Si and Mn were determined with respect to the distance from this isoconcentration surface as described in Ref. [7] and are shown in Figure 3. The concentration of Cu in the center of the Cu precipitates is 50–70 at.%, in agreement with the observations in Refs. [7,8,10–12] and the interface showed strong enrichment by Ni and Mn, similar to those found in Refs. [7,8,10]. The concentration of Co in the precipitates was much less than in the matrix, indicating that Co is rejected from the Cu precipitates into the matrix during the Cu precipitate formation.

First-principles density functional calculations were performed to estimate the effect of Co on Cu precipitate formation. The calculations of electronic structure and total energies were performed using the Vienna Ab initio Simulation Package (VASP) within a projector augmented wave (PAW) formalism [21–23] with the generalized gradient approximation for the exchange-

Table 2. Tensile and Charpy V-notch (CVN) toughness properties of 0 wt.% Co, 3 wt.% Co and 7 wt.% Co 17-4 PH alloys.

Alloy, wt.% Co	UTS, MPa	Y.S, MPa	% Elongation	CVN, J
0	1280 ± 55	1140 ± 94	7.4 ± 0.02	3.7 ± 1.8
3	1360 ± 22	1250 ± 36	9.3 ± 2.8	5.6 ± 2.3
7	1440 ± 31	1290 ± 67	9.3 ± 0.6	5.3 ± 1.5

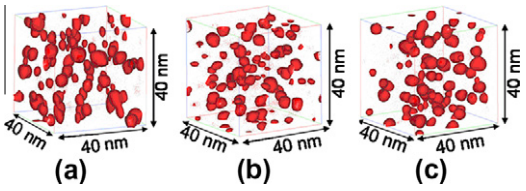

Figure 1. A 40 nm × 40 nm × 40 nm representative isosurface of Cu precipitates in (a) 0 wt.% Co 17-4 PH, (b) 3 wt.% Co 17-4 PH and (c) 7 wt.% Co 17-4 PH.

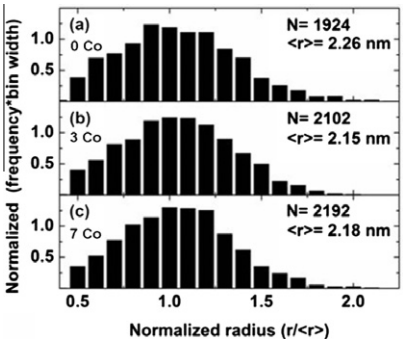

Figure 2. Normalized and scaled Cu precipitate particle size distributions in 17-4 PH steel with (a) 0 wt.% Co, (b) 3 wt.% Co and (c) 7 wt.% Co, after aging to peak hardness.

correlation functional [24]. The equilibrium lattice parameters of bcc Fe, hexagonal close-packed Co and face-centered cubic Cu calculated with $16 \times 16 \times 16$ k-points in the Brillouin zone were found to be in a good agreement with earlier experimental results [25]. The atomic interactions between Fe, Co and Cu in bcc Fe matrix were studied by comparing the total energy of 54-atom supercells with different Co and Cu substitution sites. The purpose of study of each configuration is outlined in Table 3. The substitution sites used in the models are shown in Figure 4.

Model A was used to evaluate the Cu–Cu interaction in bcc Fe (Fig. 4a). It included two Cu atoms in bcc Fe. Three configurations were compared: (i) the first nearest neighbors Cu1–Cu2, (ii) the second nearest neighbors Cu1–Cu3 and (iii) the remote Cu1–Cu4 positions. With respect to configuration (iii), the decrease in energy was 0.23 eV in configuration (i) and 0.08 eV in configuration (ii). These results demonstrate that the interaction between the first and the second nearest Cu atoms is strongly attractive in bcc Fe. Similar results have been observed in Refs. [26,27].

Model B was used to determine the atomic interaction between Cu and Co atoms in bcc Fe (Fig. 4a). Three configurations were compared: (i) the first nearest neighbors Cu1–Co2, (ii) the second nearest neighbors Cu1–Co3 and (iii) the remote Cu1–Co4 positions. The energy gain was less than 0.01 eV for all different Co locations relative to Cu; and thus, Co has no preference to occupy the sites near a Cu atom.

For models C, D and E, the Cu precipitate was modeled as a bcc-like Cu-precipitate consisting of nine Cu atoms [Cu9] inserted into bcc Fe matrix (Fig. 4b). Model C was used to determine the preference of Co to occupy a center site or corner site within a Cu precipitate present in the bcc Fe matrix. The total energy of structurally relaxed [CoCu8] Fe45 supercells and the Co–Cu distance were compared for two configurations: (i) Co in the center of the Cu-precipitate (site 2), and (ii) Co substituted for a Cu atom at the corner of the Cu-cube (site 1). We found that case (ii) was energetically more favorable by 0.80 eV as compared to case (i). The Co–Cu distance in case (i) was 2.482 Å and in case (ii) was 2.494 Å. The distance between the Fe and Co atoms in case (ii) was 2.416 Å, which is lower as compared to the Co–Cu distances. From this model, it was predicted that the formation of the strong Fe–Co bonds is the reason for the Co-in-corner configuration being energetically more favorable.

Model D was used to determine the relative preference of Fe or Co to be present in the Cu precipitate in a bcc Fe matrix. In this model [FeCu8] CoFe44, one Fe atom is in the center of the Cu-precipitate (site 2), whereas Co substituted for a remote Fe atom (site 4), i.e. Co is in the Fe matrix away from the Cu precipitate. It was observed that the configuration [FeCu8] CoFe44 in which Co substituted for Fe and was at a distance away from the Cu atoms (site 4) was lower in energy by 0.09 eV than the configuration [CoCu8] Fe45 with Co in the center site of the Cu precipitate (Model C, case (i)). This model predicts that inside a Cu precipitate, the presence of Fe atoms is energetically preferred over Co atoms.

Model E was used to determine whether Co atoms prefer to be present close to or far away from the Cu precipitate. In this model, [Cu9] Fe44Co, the bcc-like Cu precipitate [Cu9] contained neither Fe nor Co, and Co was present in the Fe matrix (i) near the nine-atom Cu cube, at the body center of an adjacent unit cell (site 5); or (ii) far from the Cu precipitate (site 4). In case (i), four Co–Fe bonds and four Co–Cu bonds were formed as compared to case (ii) where eight Co–Fe bonds were formed. The total energy of case (ii) was lower by 0.42 eV than the case (i). Hence Fe–Co bonds are more stable than the Co–Cu bonds.

Further, using the 54-atom bcc supercell, the mixing energies E_{mix} of impurity metal (Me) in bcc Fe and bcc Cu were calculated according to the following equations:

$$E_{\mathrm{mix}}(\mathrm{Me_{Fe}}) = E(\mathrm{Fe53Me}) - 53E(\mathrm{Fe}) - E(\mathrm{Me}) \quad (2)$$

$$E_{\mathrm{mix}}(\mathrm{Me_{Cu}}) = E(\mathrm{Cu53Me}) - 53E(\mathrm{Cu}) - E(\mathrm{Me}) \quad (3)$$

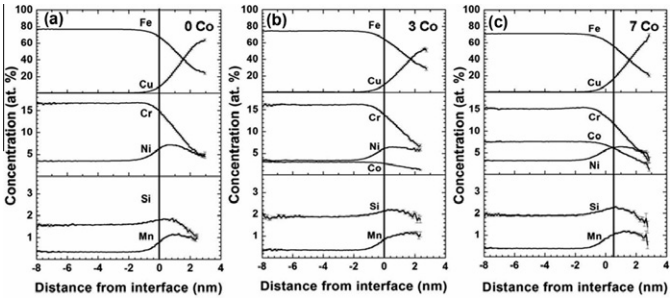

Figure 3. Proximity histogram concentration profiles of Fe, Cu, Cr, Ni, Si and Mn across the Cu precipitate–matrix interface, with respect to a 10 at.% Cu isoconcentration surface: (a) 0 wt.% Co, (b) 3 wt.% Co and (c) 7 wt.% Co.

Table 3. First-principles study of different atomic configurations of Cu and Co in bcc Fe.

Model	Purpose
A	Cu–Cu interaction
B	Cu–Co interaction
C	Preference of Co to occupy corner vs. center site in Cu precipitate
D	Preference of Fe vs. Co in Cu precipitate
E	Preference of Co to occupy a near vs. far away site from Cu precipitate

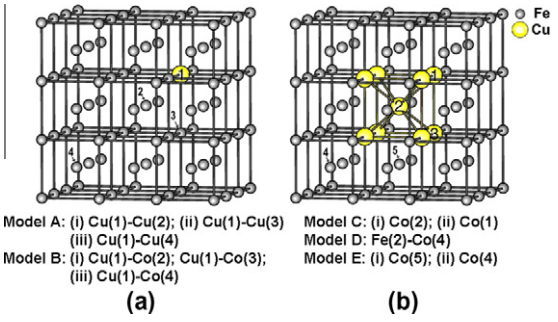

Figure 4. Atomic positions of Cu, Co and Fe in (a) Models A and B, and (b) Models C, D and E. The substitution sites are numbered in the figure. The sites substituted by atoms in each configuration are denoted in parenthesis.

where E(Fe53Me) and E(Cu53Me) are the total energies of the 54-atom supercell of bcc Fe and bcc Cu, respectively, with substituted impurity Me; and E(Fe), E(Cu) and E(Me) are the total energies of the corresponding pure metals. A large difference in mixing energies of Cu and Co in bcc Fe was observed. The E_{mix} was determined to be +0.56 eV and −0.14 eV for 1.8 at.% content of Cu and Co in bcc Fe, respectively, which correlates with the low solubility of Cu in bcc Fe and the existence of bcc Fe–Co solid solutions up to ~75 at.% Co as observed in the Fe–Co phase diagram [28]. The mixing energies of 1.8 at.% Fe and 1.8 at.% Co in bcc Cu are both positive, +0.21 eV and +0.48 eV, respectively, which is in accord with the limited solubility of both Fe and Co in Cu.

From the above models and mixing energies, it is observed that in Fe–Co–Cu system, Co has a strong tendency to form strong Fe–Co bonds. Hence, during thermal aging, it is expected that Co would be rejected from the Cu precipitate to the interface and matrix, and over time this would result in a lower concentration of Co in the Cu precipitate as compared to the interface and matrix. The lower concentration of Co in the Cu precipitate as compared to the matrix observed using APT (Fig. 3b and c) is hence explained.

In summary, APT in conjunction with first-principles studies have been used to investigate Cu precipitation in 17-4 PH steel. The average radius of the Cu precipitates is statistically significantly lower in the Co-alloyed 17-4 PH steel as compared to the steel with no Co. The distribution of Cu precipitate radii narrowed with Co addition and Co is rejected out of the Cu precipitate during precipitate formation. Therefore, it is concluded that the presence of Co significantly affects the size and size distribution. The first-principles study shows that the tendency to form strong Fe–Co bonds leads to rejection of Co from Cu precipitates.

The authors would like to thank Benet Laboratories for funding this work and NUCAPT facility at Northwestern University for the local electrode atom probe work.

[1] E. Hornbogen, R.C. Glenn, Trans. Metall. Soc. AIME 218 (1960) 1064–1070.
[2] S.R. Goodman, S.S. Brenner, J.R. Low Jr., Metall. Trans. 4 (1973) 2363–2369.
[3] P.J. Othen, M.L. Jenkins, G.D.W. Smith, Philos. Mag. A 70 (1994) 1–24.
[4] S.R. Goodman, S.S. Brenner, Metall. Trans. 4 (1973) 2371–2378.
[5] R. Carter, N. Soneda, K. Dohi, J. Hyde, C. English, W. Server, J. Nucl. Mater. 298 (2001) 211–224.
[6] M.K. Miller, B.D. Wirth, G.R. Odette, Mater. Sci. Eng. A 353 (2003) 133–139.
[7] D. Isheim, R.P. Kolli, M.E. Fine, D.N. Seidman, Scripta Mater. 55 (2006) 35–40.
[8] M.D. Mulholland, D.N. Seidman, Acta Mater. 59 (2011) 1881–1897.
[9] R.P. Kolli, D.N. Siedman, Acta Mater. 56 (2008) 2073–2088.
[10] D. Isheim, M.S. Gagliano, M.E. Fine, D.N. Seidman, Acta Mater. 54 (2006) 841–849.
[11] D. Isheim, D.N. Siedman, Surf. Interface Anal. 36 (2004) 569–574.
[12] M. Murayama, Y. Katayama, K. Hono, Metall. Mater. Trans. A 30A (1999) 345–353.
[13] G.R. Speich, D.S. Dabowski, L.F. Porter, Metall. Trans. 4 (1973) 303–315.
[14] K.J. Irvine, D.T. Llewellyn, F.B. Pickering, J. Iron Steel Int. (1959) 218.
[15] D. Coutsourdais, Mem. Rev. De Metallurgie 58 (1961) 503–509.
[16] A.S. Murthy, S. Lekakh, V.L. Richards, D. Van Aken, Proceedings of Symposia Held During the TMS Annual Meeting and Exhibition, Wiley, Hoboken, NJ, 2011, pp. 651–658.
[17] B. Gault, D. Haley, F. de Geuser, M. Moody, E. Marquis, D. Larson, B. Geiser, Ultramicroscopy 111 (2011) 448–457.
[18] O.C. Hellman, J.A. Vandenbrouke, J. Rusing, D. Isheim, D.N. Seidman, Microsc. Microanal. 6 (2000) 437–444.
[19] F. Vurpillot, A. Bostel, D. Blavette, Appl. Phys. Lett. 76 (2000) 3127–3129.
[20] M.K. Miller, E.A. Kenik, Microsc. Microanal. 10 (2004) 336–341.
[21] G. Kresse, J. Furthmüller, Phys. Rev. B 54 (1996) 11169.
[22] G. Kresse, D. Joubart, Phys. Rev. B 59 (1999) 1758.
[23] G. Kresse, J. Hafner, J. Phys. Condens. Matter 6 (1994) 8245–8257.
[24] J.P. Perdew, K. Burke, M. Ernzerhof, Phys. Rev. Lett. 77 (1996) 3865–3868.
[25] C. Kittel, Introduction to Solid State Physics, Wiley, New York, 1996.
[26] F. Soisson, C.-C. Fu, Phys. Rev. B 76 (2007) 214102.
[27] O.I. Gorbatov, A.V. Ruban, P.A. Korzhavyi, Y.N. Gornostyrev, Mater. Res. Soc. Symp. Proc. 1193 (2009) 469.
[28] T. Nishizawa, K. Ishida, Co–Fe binary alloy phase diagrams, ASM Handbooks Online, ASM International, 1984.